Proceedings of the ASME 2018
Conference on Smart Materials, Adaptive Structures and Intelligent Systems
SMASIS2018
September 10-12, 2018, San Antonio, TX, USA

SMASIS2018-8004

EXPERIMENTAL STUDY OF MULTIFUNCTIONAL NCM-SI BATTERIES WITH SELF-ACTUATION

Jun Ma
Mechatronics Research Laboratory
Department of Mechanical and Nuclear Engineering
The Pennsylvania State University
University Park, Pennsylvania 16802
Email: jxm1153@psu.edu

Cody Gonzalez
Department of Mechanical and Nuclear Engineering
The Pennsylvania State University
University Park, Pennsylvania 16802
Email: cag46@psu.edu

Christopher Rahn*
Professor
Mechatronics Research Laboratory
Department of Mechanical and Nuclear Engineering
The Pennsylvania State University
University Park, Pennsylvania 16802
Email: cdrahn@psu.edu

Mary Frecker
Professor
Department of Mechanical and Nuclear Engineering
The Pennsylvania State University
University Park, Pennsylvania 16802
Email: mxf36@psu.edu

Donghai Wang
Associate Professor
Energy Nanostructure Laboratory
Department of Mechanical and Nuclear Engineering
The Pennsylvania State University
University Park, Pennsylvania 16802
Email: dwang@psu.edu

ABSTRACT

Among anode materials for lithium ion batteries, silicon (Si) in known for high theoretical capacity and low cost. Si exhibits over 300% *volume change during cycling, potentially providing large displacement. In this paper, we present the design, fabrication and testing of a multifunctional NCM-Si battery that not only stores energy, but also utilizes the volume change of Si for actuation. The battery is transparent, thus allowing the visualization of the actuation process during cycling. This paper shows Si anode design that stores energy and actuates through volume change associated with lithium insertion. Experimental results from a transparent battery show that a Cu current collector single-side coated with Si nanoparticles can store* $10.634\,mWh$ *(charge)/* $2.074\,mWh$ *(discharge) energy and bend laterally with over* 40% *beam length displacement. The unloaded anode is found to remain circular shape during cycling. Using a unimorph cantilever model, the Si coating layer actuation strain is estimated to be* 30% *at* 100% *SOC.*

INTRODUCTION

Among anode materials for lithium ion batteries, Si is known for its high theoretical capacity ($4200\,mAh/g$ [1] compared to graphites $372\,mAh/h$ [2]), making it an ideal option for high energy density applications such as portable electronics, electric vehicles and drones [3] [4]. Si shows over 300% volume change during cycling [5], potentially providing large displacement for actuation. As shown in Table 1, Si's Young's modulus is comparable to piezoelectric ceramic and shape memeory alloy and much higher than electrostrictive polymer, while

*Address all correspondence to this author.

TABLE 1. COMPARISON BETWEEN SI AND POPULAR ACTUATOR MATERIALS [9] [10] [11] [12] [13]

	Maximum actuation strain	Young's modulus (GPa)	Maximum frequency (Hz)
Si	45%	$20-90$	$<3\times10^{-3}$
Piezoelectric ceramic	$0.005\%-0.02\%$	$50-300$	$5\times10^{5}-3\times10^{7}$
Piezoelectric polymer	$0.02\%-0.1\%$	$2-10$	$1\times10^{5}-1\times10^{7}$
Shape memory alloy	$0.7\%-7\%$	$30-90$	$2\times10^{-2}-7\times10^{0}$
Electrostrictive polymer	4%	0.38	$1\times10^{2}-1\times10^{6}$

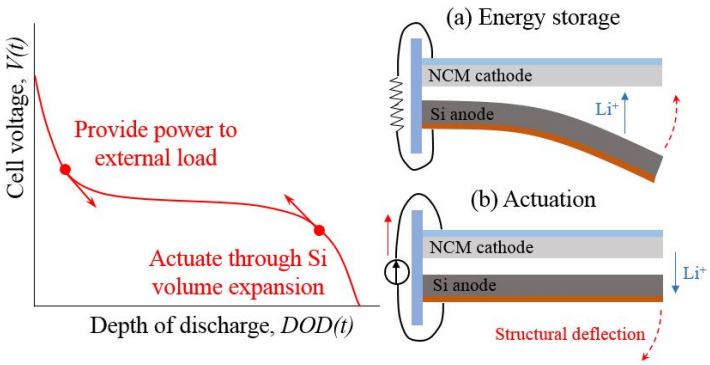

FIGURE 1. MULTIFUNCTIONAL NMC-SI BATTERY CONCEPT: (A) ENERGY STORAGE AND POWER SUPPLY TO EXTERNAL LOAD; (B) ACTUATION WITH STRUCTURAL DEFLECTION DURING CHARGING

providing higher strain, so the potential exists for high actuation energy density. Due to relatively reluctant ionic transportation in Li-ion batteries, the actuation speed of Si is slow compared with other materials. Although the high volume change of Si may result in actuation fatigue and fast capacity fade [6], researchers found that using small Si particles (<100 nm) in a compliant,conductive matrix can improve battery performance and reduce cracking [7] [8].

As discussed in [14], Fig. 1 shows the concept of the multifunctional battery. Si as battery anode active material is single-side coated on a Cu current collector. A substrate clamps one end of the anode and leaves the other end free to move, forming a unimorph cantilever configuration. The Si anode is paired with a $Li(Ni_{0.5}Co_{0.2}Mn_{0.3})O_2$ (NCM) cathode. Soaked in electrolyte, the pair is able to store energy during charge and provide power to external load during discharge. During charge, Li ions migrate from the cathode, through the electrolyte and insert in

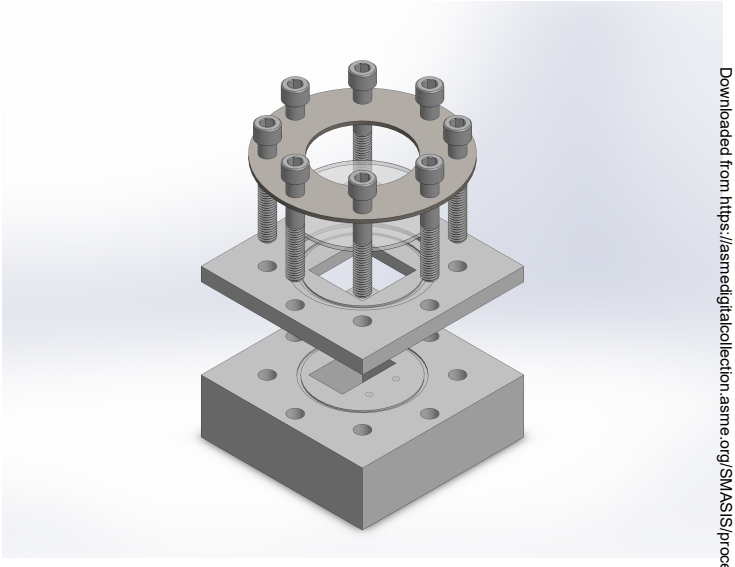

FIGURE 2. TRANSPARENT BATTERY DESIGN

the Si anodes, causing coating layer to expand. With the Cu current collector constraining axial motion, the anodes deform away from the cathode. During discharge, Li ions migrate back to cathode, reversing the bending motion. Thus, the electrode shape is dependent on battery state of charge (SOC).

In this paper, we present the design, fabrication and testing of a transparent battery that allows measurement of voltage, current and anode bending displacement. The battery's electrochemical performance is tested in coin cells and anode motion is captured with a digital camera. A unimorph composite beam model is presented to predict the volume expansion mechanism of the porous coating structure as well as the relationship between anode tip deflection and battery SOC.

MULTIFUNCTIONAL BATTERY DESIGN AND FABRICATION

Fig. 2 shows the transparent battery design. The battery consists of two polypropylene (PP) pieces. The upper piece is $15.24\,cm\times15.24\,cm\times1.27\,cm$. It has a $\varnothing10.16\,cm\times0.32\,cm$ circular step to fit a borosilicate glass disc and a $5.08\,cm\times5.08\,cm\times0.95\,cm$ concentric cut-through hole. The lower piece is $15.24\,cm\times15.24\,cm\times5.08\,cm$. It has a $5.08\,cm\times3.18\,cm\times3.81\,cm$ test chamber where the battery core is located. To seal the contact surfaces between the glass disc and the upper piece and between the upper and the lower pieces, two O-ring grooves ($8.78\,cm\,OD\times8.26\,cm\,ID\times0.13\,cm$) are machined on both sides of the upper piece. The O-rings ($8.57\,cm\,OD\times8.26\,cm\,ID\times0.18\,cm$) are FEP-encapsulated with silicon core which offer chemical compatibility with battery electrolyte. When the eight

nuts are tightened, the O-rings are pushed into the grooves to provide good sealing.

The battery core consists of one NCM cathode and four Si anodes. The NCM cathode coating consists of NCM particles ($94.2\,wt\%$, average particle diameter around $10\,\mu m$), polyvinylidene fluoride (PVDF) binder ($2.9\,wt\%$) and carbon black (CB) conductive additive ($2.9\,wt\%$). The single-sided coating is nominally $44\,\mu m$ thick and the Al current collector is $15\,\mu m$ thick. The NCM active material loading is $12.1\,mg/cm^2$. The cathode ($3.5\,cm \times 3.5\,cm$) is inserted into a separator pouch which provides insulation from the anodes while allowing lithium ions travel through. The pouch is made of two pieces of Celgard 2320 separator ($4.0\,cm \times 4.0\,cm \times 20\,\mu m$). The separators are heat sealed on three edges. The last edge is left open for cathode insertion and electrical connection. An Al wire serves as the positive terminal, connecting to the NCM cathode through resistance welding.

To fabricate anodes, Si nanoparticles ($60\,wt\%$, average particle diameter around $50\,nm$), polyacrylic acid (PAA) binder ($20\,wt\%$) and CB conductive additive ($20\,wt\%$) are dissolved in deionized water to form a uniform slurry. The slurry is then coated on a $34\,\mu m$ thick Cu current collector. After drying, the coating layer forms a porous structure. The average coating thickness is $6\,\mu m$. The Si loading is $0.566\,mg/cm^2$. The coated sheet is then cut into four $3\,cm \times 4\,mm$ strips. One end of each anode is connected to a 24 gauge Cu wire through resistance welding. The Cu wires are polytetrafluoroethylene (PTFE) insulated, allowing us to measure anode potentials individually. Two of the four anodes have $56.320\,mg$ Ni proof mass attached to their free ends. The electrodes are attached to a PP substrate with Loctite E-120HP Hysol epoxy, as shown in Fig. 3. This setup is then installed onto the side wall of the test chamber with the same epoxy. The prototype battery before electrolyte filling is shown in Fig. 4.

The entire device is dried in a vacuum oven at $60\,^{\circ}C$ for 24 hours prior to moving into a glovebox for electrolyte filling. The electrolyte is 1M $LiPF_6$ in ethylene carbonate (EC) and ethyl methyl carbonate (EMC) solution (1:1 by volume). The electrolyte is added through a filling port located on the side wall of the lower PP piece. After filling, the filling port is sealed with a chemical resistant plug. With this design, the anodes are free to deform inside the test chamber and we are able to observe and measure electrode deflection and battery voltage from outside.

TEST SETUP

The device is tested on a Landt A2000 coin cell tester at room temperature. During electrochemical testing, the four anodes are cycled together using one channel from the tester. To ensure even current distribution between the anodes, the four Cu wires are first connected to a bus bar and then connected to the tester. The charge and discharge cycles are performed with constant current at approximately C/20 rate (meaning a battery at 100% SOC can be fully discharged in 20 hours, with current being $0.26\,mA$). To ensure the anode deflections are within material elastic region, the cell is not fully charged to the cutoff voltage ($4.20\,V$). The device rests for $5\,min$ followed by constant current discharge when the anode deflections are monitored. During the test, the electrodes and substrate are oriented vertically so gravity has minimal effect on electrode shape. A digital camera with a macro lens is used to capture the deformation process. One picture is taken every 30 seconds. The test setup is shown in Fig.

FIGURE 3. ELECTRODE SETUP: NCM CATHODE IN A SEPARATOR POUCH AND FOUR SI ANODES FACING TOWARD THE CATHODE

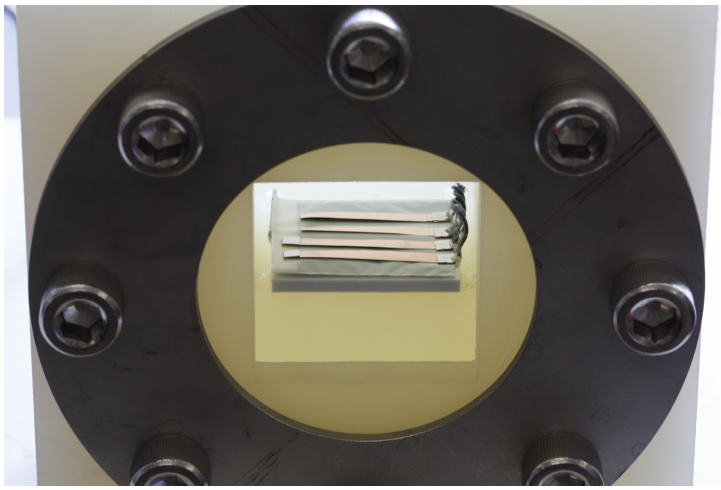

FIGURE 4. TRANSPARENT BATTERY PROTOTYPE: ELECTRODE SETUP IN TEST CHAMBER BEFORE DRYING

5.

UNIMORPH CANTILEVER MODEL

To characterize Si coating layer actuation strain, a unimorph cantilever model is developed using anode tip deflection as input. Image processing provides measured data of anode tip displacement with respect to time. It is observed that the unloaded anodes bend in approximately circular shape during the test, indicating their curvature can be regarded as a constant value along beam length and the gravitational effect on beam shape is negligible. The following geometry relationship helps us to determine anode curvature from tip deflection,

$$2Rsin^2\left(\frac{\theta}{2}\right) = d, \tag{1}$$

where R is radius of curvature, d is anode tip displacement, $\theta = L/R$ is the central angle and L is anode arc length. Rearranging Eq. 1,

$$\frac{d}{R} + cos\left(\frac{L}{R}\right) - 1 = 0. \tag{2}$$

Fig. 6 shows a schematic diagram of single-side coated Si anode. To calculate the actuation strain of the Si coating layer as a function of battery SOC, we assume: (1) coating layer expansion in y and z directions are neglected; (2) the coating layer is regarded as a continuous and uniform material and its material properties are not dependent on lithium concentration; (3) the coating layer has no axial motion relative to the current collector.

The equilibrium conditions of the beam

$$N_{ct} = N_{Cu} = N, \tag{3}$$

where N_{ct} and N_{Cu} are axial forces of anode coating and copper current collector. The moment balance of the beam

$$M_{ct} + M_{Cu} = \frac{N}{2}\left(h_{ct} + h_{Cu}\right), \tag{4}$$

where M_{ct} and M_{Cu} are bending moment of coating layer and copper layer, h_{ct} and h_{Cu} are their thicknesses, respectively. Assuming cantilever curvature is κ, the bending moments

$$M_{ct} + M_{Cu} = \kappa\left(E_{ct}I_{ct} + E_{Cu}I_{Cu}\right), \tag{5}$$

TABLE 2. PARAMETERS OF SI ANODE

Parameter	Si coating layer	Cu current collector
Thickness (m)	6×10^{-6}	34×10^{-6}
Length (m)	3×10^{-2}	3×10^{-2}
Width (m)	4×10^{-3}	4×10^{-3}
Young's modulus (GPa)	1	90

where E_{ct} and E_{Cu} are Young's modulus, I_{ct} and I_{Cu} are cross-sectional moment of inertia, which can be determined with parallel axis theorem,

$$I_{ct} = \frac{1}{12}Wh_{ct}^3 + Wh_{ct}\left(\frac{h_{ct}}{2} + h_{Cu} - h_n\right)^2, \tag{6}$$

$$I_{Cu} = \frac{1}{12}Wh_{Cu}^3 + Wh_{Cu}\left(h_n - \frac{h_{Cu}}{2}\right)^2, \tag{7}$$

where h_n is the position of neutral axis,

$$h_n = \frac{E_{Cu}\frac{h_{Cu}^2}{2} + E_{ct}h_{ct}\left(h_{Cu} + \frac{h_{ct}}{2}\right)}{E_{Cu}h_{Cu} + E_{ct}h_{Cu}}. \tag{8}$$

The non-slip interface condition can be written as

$$S^* - \frac{N_{ct}}{E_{ct}A_{ct}} - \kappa\frac{h_{ct}}{2} = \frac{N_{Cu}}{E_{Cu}A_{Cu}} + \kappa\frac{h_{Cu}}{2}, \tag{9}$$

where S^* is the actuation strain of Si coating layer due to Li insertion. Combining Eqs. 3 4 5 9, we obtain the actuation strain

$$S^* = \kappa\left[\frac{2(E_{ct}I_{ct} + E_{Cu}I_{Cu})}{h_{ct} + h_{Cu}}\left(\frac{1}{E_{ct}A_{ct}} + \frac{1}{E_{Cu}A_{Cu}}\right) + \frac{h_{ct} + h_{Cu}}{2}\right]. \tag{10}$$

Table 2 shows the parameters used in calculation.

RESULTS AND DISCUSSION

The electrochemical performance of the transparent battery is shown in Fig. 7. 14 cycle tests were conducted with constant current. In first 6 cycles, the charge cutoff voltage was gradually increased from $3.78\,V$ to $4.00\,V$. In last 8 cycles, the charge cutoff voltage was fixed at $4.00\,V$. The discharge cutoff voltage

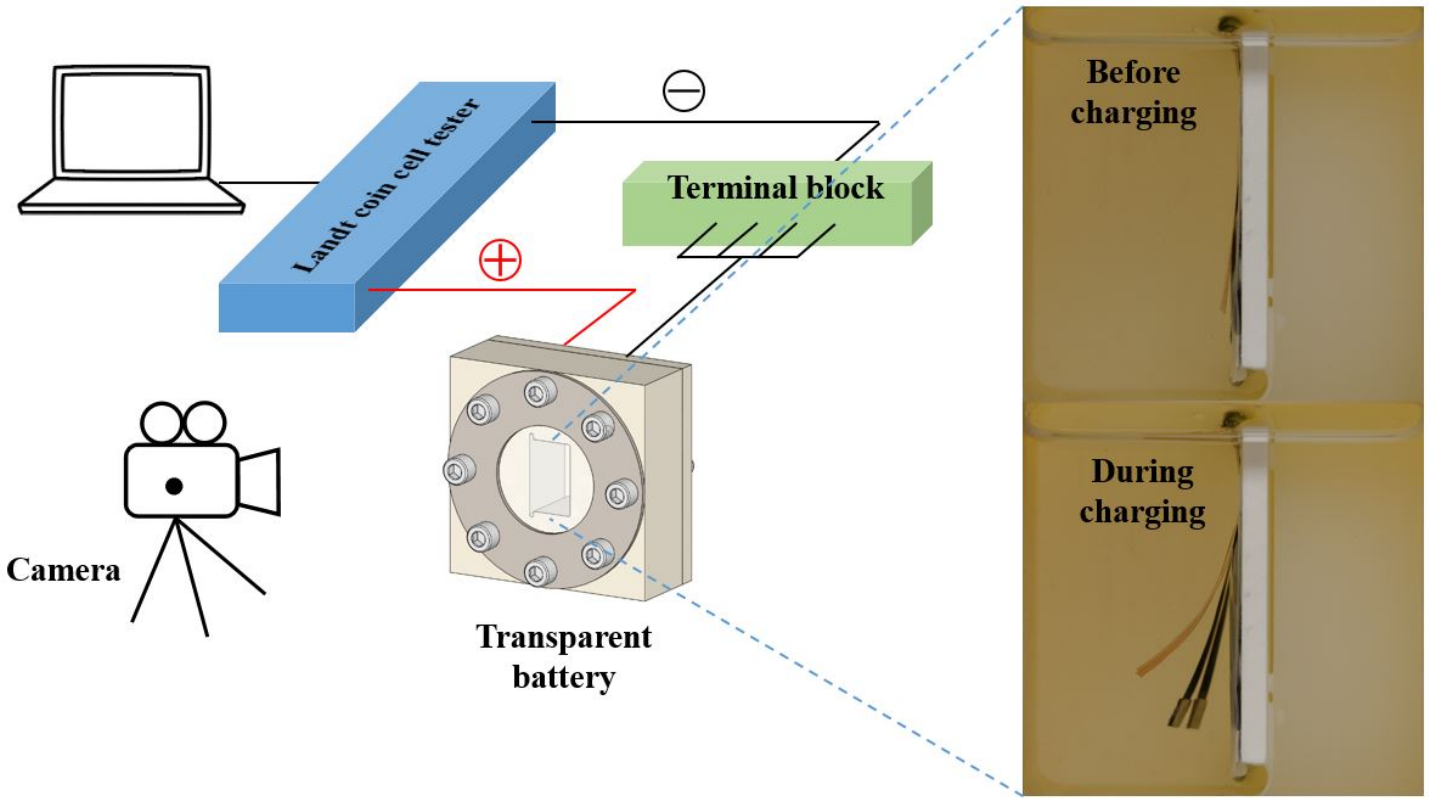

FIGURE 5. TEST SETUP FOR TRANSPARENT BATTERY

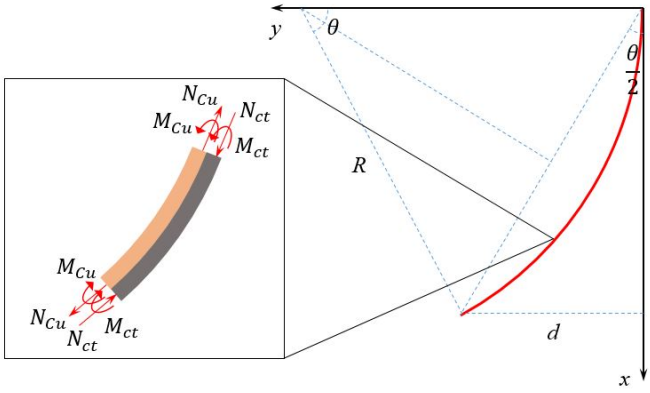

FIGURE 6. GEOMETRY RELATIONSHIP BETWEEN ANODE TIP DISPLACEMENT AND CURVATURE AND UNIMORPH CANTILEVER FREE BODY DIAGRAM

was $2.00\,V$ for all cycles.

From charge and discharge curves in Fig. 7(A), we see that the transparent battery is storing energy during charging from less than $2.0\,V$ to over $3.7\,V$. The stored energy is recovered during a subsequent discharge. The transparent battery sources $2\,mWh$ during the first cycle and peaks at $3\,mWh$ in cycle 6. The cell expresses significant capacity loss in the first cycle (charge capacity is 3.132 mAh and discharge capacity is 0.677 mAh, with capacity loss being 78.4%). The low cycle efficiency is attributed to two effects: (1) The first lithiation process of Si is associated with phase transition from crystal Si to amorphous Si [6]. The phase transition is associated with plastic deformation so the anodes do not fully return to their initial position, leaving a gap between the anodes and the cathode. The gap significantly slows liquid phase ionic transport. Liquid phase diffusion time constant for Li ions can be written as $\tau = L^2/D$, where L is diffusion distance and $D = 2.6 \times 10^{-10}\,m^2/s$ is Li ion diffusivity in electrolyte. For gap $L = 5 \times 10^{-3}\,m$ between cathode and anode, the characteristic time $\tau = 96154\,s$. Such large time constant indicates Si active material close to the beam tip has lost cycling capability. Only material close to the base exhibits normal cycling; (2) When Si is first lithiated, a solid-electrolyte interphase (SEI) forms on the outer surfaces of the Si particles. The SEI consists of inorganic crystals electrochemically reduced

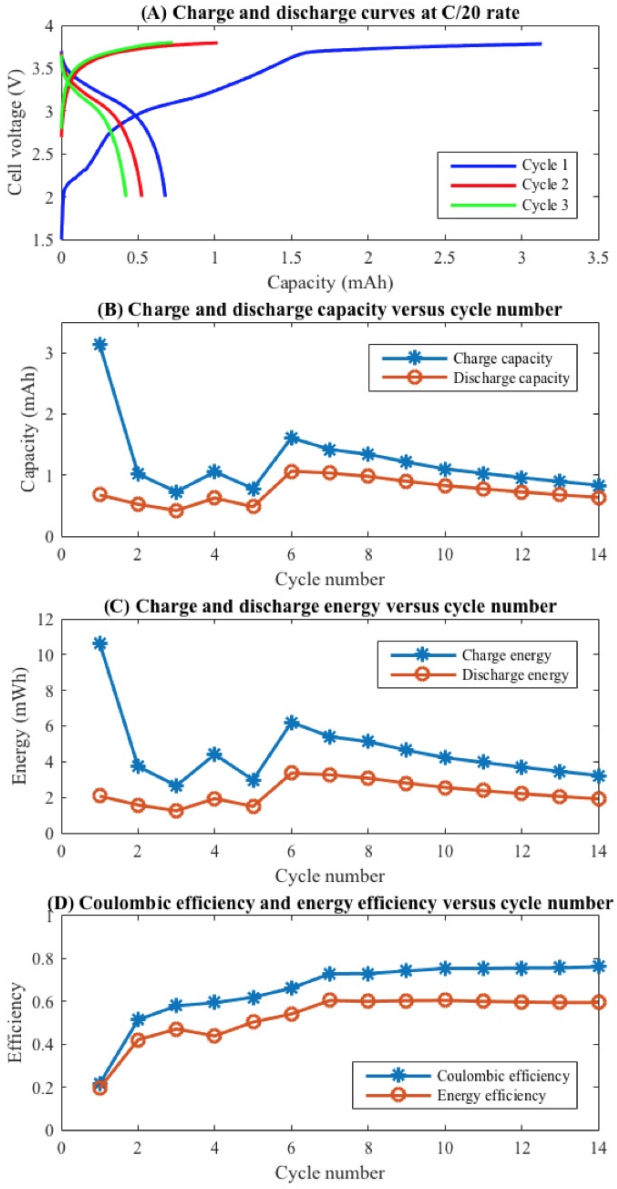

FIGURE 7. EXPERIMENTAL ELECTROCHEMICAL PERFORMANCE OF THE TRANSPARENT BATTERY

from solvent and electrolytic salt [6]. The Si nanoparticles used in the anode coating provide a large surface area for this reaction, which irreversibly consumes Li ions.

As shown in Fig. 7(D), both coulombic efficiency and energy efficiency increase gradually from cycle 1 to cycle 6 and stabilizes around cycle 7. This is possibly due to the fixed charge cutoff condition and completion of SEI formation. The coulombic efficiency is around 75% and the energy efficiency is around 60%. The values are significantly lower than a NCM-Si coin

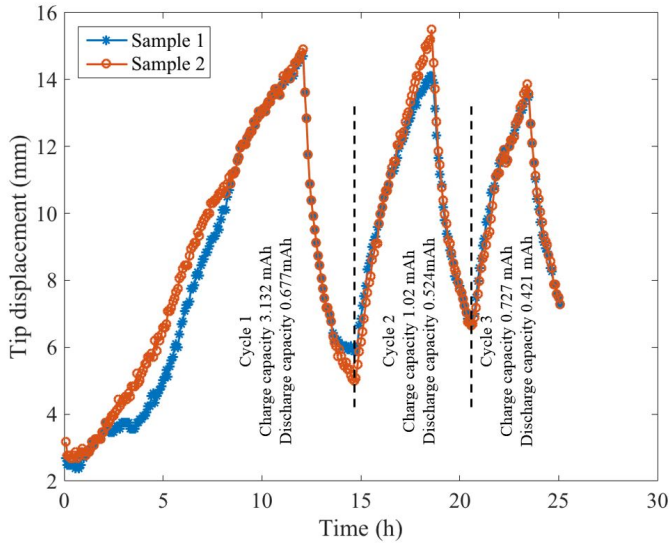

FIGURE 8. EXPERIMENTAL TIP DISPLACEMENT OF UNLOADED ANODES IN FIRST THREE CYCLES

cell, whose coulombic and energy efficiency are expected to be greater than 90% and 80%, respectively.

The tip displacement of the unloaded anodes in the first 3 cycles is shown in Fig. 8. The tip displacement is nonzero at the beginning of the test, due to binder swelling effect after electrolyte filling. The tip displacement increases slowly with battery SOC in first 5 hours. For the porous coating layer, the expanding Si particles occupy pores first. This phenomenon is only observed in the first cycle, indicating it is an irreversible process. After each cycle, the anode tip does not return to its initial position, indicating the deformation consists of elastic deformation as well as plastic deformation. In the first cycle, the two anodes show different tip displacement, possibly due to uneven coating. For Sample 1, its tip moves back and forth in first 5 hours, indicating rearrangement of the porous coating layer. With Sample 1 being closer to the cathode, it attracts more Li ions than Sample 2 because of a shorter diffusion distance. The result is self-balancing phenomenon that allows Sample 1 to catch up with Sample 2 and eventually reach the same tip displacement.

The unloaded anodes are observed to maintain approximately circular shape (constant curvature along beam length) during cycling. The shape validation is shown in Fig. 9. The solid lines are constant curvature arcs calculated with anode tip deflection at 20%, 40% and 60% battery SOC, respectively. The stars are anode shape sample points extracted from digital im-

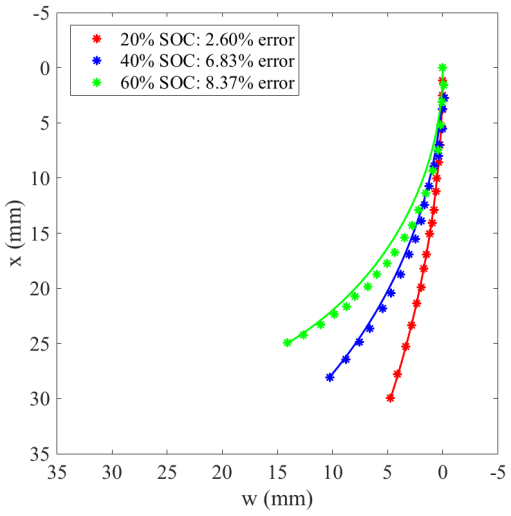

FIGURE 9. COMPARISON OF EXPERIMENTAL MEASURED ANODE SHAPE (STAR) AND ARC CALCULATED WITH TIP DEFLECTION (SOLID LINE) AT DIFFERENT BATTERY SOC

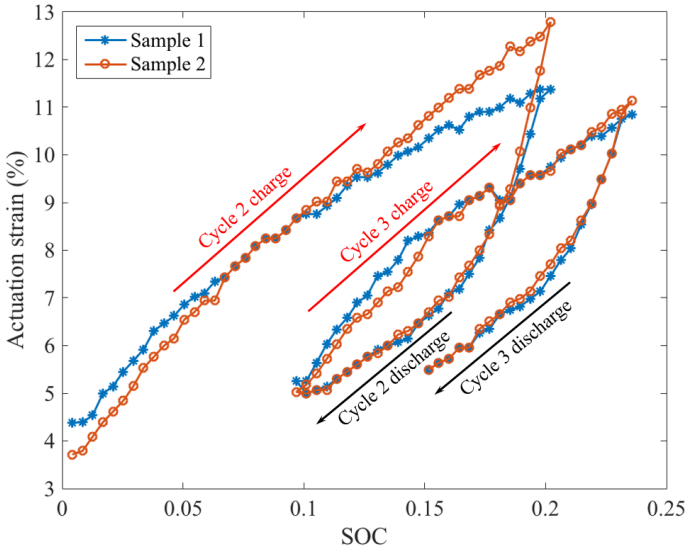

FIGURE 10. ACTUATION STRAIN OF ANODE COATING LAYER IN THE SECOND AND THIRD CYCLE

ages. The error

$$err = \frac{\sqrt{\sum (w_{sample} - w_{arc})^2}}{\sqrt{\sum w_{sample}^2}}, \tag{11}$$

is smallest at low SOC and remains below 10% for all cases, showing the circular shape assumption is reasonable.

The actuation strain of the coating layer in the second and third cycle is calculated from tip displacement data using a unimorph cantilever model. As shown in Fig. 10, the actuation strain exceeds 7% at less than 20% battery SOC. Assuming the strain has a linear relationship with battery SOC, over 30% strain can be expected when battery is fully charged. The hysteresis of the actuation curve is due to SEI formation and plastic deformation of Si particles, as discussed above. The actuation strain is closely related to coating layer thickness, porosity and composition. By adjusting these electrode design factors, we are able to tune actuation and energy storage performance. Note that only positive strain is achieved with unimorph cantilever design. To make electrode deform in both directions, we can double side coat Cu current collectors with Si to form a bimorph configuration.

CONCLUSION

This paper shows Si anode design that stores energy and actuates through volume change associated with lithium insertion. Experimental results from a transparent battery show that a Cu current collector single-side coated with Si nanoparticles can store 10.634 mWh (charge)/ 2.074 mWh (discharge) energy and bend laterally with over 40% beam length displacement. The unloaded anode is found to remain circular shape during cycling. Using a unimorph cantilever model, the Si coating layer actuation strain is estimated to be 30% at 100% SOC.

The actuation process introduces a large gap between cathode and anode, resulting in reduced battery performance. In future tests, battery cathode and anode should deform together to keep the gap small and constant. With Si particles double-side coated on Cu current collector, the bimorph anode has the potential to demonstrate axial deformation when its two sides are lithiated simultaneously. The electrode has hollow pattern to maximize the deformation. The new design will be experimentally studied in transparent battery and analytically modeled.

Since the actuation strain is based on experimental data, the result depends on measurement accuracy and test repeatability. For example, Si coating layer thickness may not be uniform across anode length due to imperfect fabrication. Further tests are still needed to validate the results. Besides, in the unimorph cantilever model, the coating layer homogeneous modulus is assumed to be constant. However, as Si particles expand, the coating layer porosity and composite volume fraction are also changing. Therefore, a more detailed analysis of coating layer modulus as a function of battery SOC is needed.

ACKNOWLEDGMENT

The material is based upon work supprted by National Science Foundation under Grant No. 1662055.

REFERENCES

[1] Obrovac, M. N., and Christensen, L., 2004. "Structural changes in silicon anodes during lithium insertion/extraction". *Electrochemical and Solid-State Letters,* ***7***(5), pp. A93–A96.

[2] Tarascon, J. M., and Armand, M., 2001. "Issues and challenges facing rechargeable lithium batteries". *Nature,* ***414***(6861), pp. 359–367.

[3] Scrosati, B., Hassoun, J., and Sun, Y. K., 2011. "Lithium-ion batteries. a look into the future". *Energy & Environmental Science,* ***414***(6861), pp. 3287–3295.

[4] Kempton, W., 2004. "Electric vehicles: Driving range". *Nature Energy,* ***1***, p. 16131.

[5] Beaulieu, L. Y., Eberman, K. W., Turner, R. L., Krause, L. J., and Dahn, J. R., 2001. "Colossal reversible volume changes in lithium alloys". *Electrochemical and Solid-State Letters,* ***4***(9), pp. A137–A140.

[6] McDowell, M., Lee, S., Nix, W., and Cui, Y., 2013. "25th anniversary article: understanding the lithiation of silicon and other alloying anodes for lithium-ion batteries". *Advanced Materials,* ***25***(36), pp. 4966–4985.

[7] Yi, R., Dai, F., Gordin, M., Sohn, H., and Wang, D., 2013. "Influence of silicon nanoscale building blocks size and carbon coating on the performance of microsized sic composite liion anodes". *Advanced Energy Materials,* ***3***(11), pp. 1507–1515.

[8] Song, J., Chen, S., Zhou, M., Xu, T., Lv, D., Gordin, M., Long, T., Melnyk, M., and Wang, D., 2014. "Microsized siliconcarbon composites composed of carbon-coated sub-10 nm si primary particles as high-performance anode materials for lithium-ion batteries". *Journal of Materials Chemistry A,* ***2***(5), pp. 1257–1262.

[9] Shenoy, V., Johari, P., and Qi, Y., 2010. "Elastic softening of amorphous and crystalline lisi phases with increasing li concentration: a first-principles study". *Journal of Power Sources,* ***195***(19), pp. 6825–6830.

[10] Berla, L., Lee, S., Cui, Y., and Nix, W., 2015. "Mechanical behavior of electrochemically lithiated silicon". *Journal of Power Sources,* ***273***, pp. 41–51.

[11] Huber, J., Fleck, N., and Ashby, M., 1997. "The selection of mechanical actuators based on performance indices". *Proceedings of the Royal Society of London A: Mathematical, Physical and Engineering Sciences,* ***453***(1965), pp. 2185–2205.

[12] Zhang, Q., Bharti, V., and Zhao, X., 1998. "Giant electrostriction and relaxor ferroelectric behavior in electron-irradiated poly (vinylidene fluoride-trifluoroethylene) copolymer". *Science,* ***280***(5372), pp. 2101–2104.

[13] Pelrine, R., Kornbluh, R., Joseph, J., Heydt, R., Pei, Q., and Chiba, S., 2000. "High-field deformation of elastomeric dielectrics for actuators". *Materials Science and Engineering: C,* ***11***(2), pp. 89–100.

[14] Ma, J., Rahn, C., and Frecker, M., 2017. "Multifunctional nmc-si batteries with self-actuation and self-sensing". *ASME 2017 Conference on Smart Materials, Adaptive Structures and Intelligent Systems, Snowbird, Utah, USA*.